Design for a High-resolution Small-Animal SPECT System Using Pixellated Si(Li) Detectors for *In Vivo* ^{125}I Imaging

W.-S. Choong, *Member, IEEE*, W. W. Moses, *Senior Member, IEEE*, C. S. Tindall, and P. N. Luke

***Abstract*— We propose a design for a high-resolution SPECT system for *in vivo* ^{125}I imaging in small animal using pixellated lithium-drifted silicon (Si(Li)) detectors. The detectors have high detection efficiency (>90%), good energy resolution (<15% FWHM), and good intrinsic spatial resolution (~1 mm FWHM). The SPECT system has a dual head detector geometry with the distance between the detectors ranging 30-50 mm to minimize the imaging distance between the mouse and the detectors. The detectors, each with an active area of 64 mm × 40 mm (64 × 40 array of 1 mm^2 pixels and a 6 mm thick Si(Li) detector), are mounted on a rotating gantry with an axial field-of-view of 64 mm. Using a high-resolution parallel-hole collimator, the expected spatial resolution is 1.6 mm FWHM at an imaging distance of 20 mm, and sensitivity is 6.7 cps/μCi. ^{125}I is a readily available radioisotope with a long half-life of 59.4 days and it is commonly used to label biological compounds in molecular biology. Conventional gamma cameras are not optimized to detect the low emission energies (27 to 35 keV) of ^{125}I. However, Si(Li) detector provides an ideal solution for detecting the low-energy emissions of ^{125}I. In addition, a SPECT system based on Si(Li) detectors can potentially be less expensive than other detector technology because of its ease of operation and the availability of many resources for processing silicon. This will increase the availability of small-animal SPECT systems in biomedical research, thereby providing an important tool to facilitate biological research.**

***Index Terms*— small-animal, SPECT, lithium-drifted silicon (Si(Li)), pixellated detector, iodine-125, *in vivo*.**

I. Introduction

IN recent years, small animal imaging has been the subject of intense research and development. This is largely due to the advances in molecular and cell biology, the use of transgenic mice models and the availability of new imaging tracers. The genetic similarity of mice to humans has enabled a wide range of human diseases to be studied in animal models. The completion of the sequence of the human genome [1] and mouse genome [2] will improve our understanding of human biology at the molecular level, and create new and improved models of human diseases. Transgenic mice have been widely used in the study of cancer mechanisms and for modeling human diseases. Recently, the study of transgenic mice has opened new prospects in evaluating human gene therapy by noninvasive, repetitive and quantitative imaging of gene expression. Study methods for small animals include [3]: (1) imaging gene expression and regulation to reflect specific cellular and molecular processes; (2) imaging cell trafficking to understand the molecular pathways of many diseases; and (3) imaging during gene therapy to assess the effectiveness of the gene transduction.

Manuscript received Nov 15, 2003. This work was supported in part by the U.S. Department of Energy under contract No. DE-AC03-76SF00098.

The authors are with the Lawrence Berkeley National Laboratory, Berkeley, CA 94720 USA (telephone: 510-486-6757, e-mail: wschoong@lbl.gov).

II. ^{125}I Imaging in Small Animals

One of the most common single-photon radioisotopes used in human nuclear imaging is ^{99m}Tc, which emits a single 140 keV photon. As a result, conventional gamma cameras are optimized to detect the emissions from ^{99m}Tc. However, for small-animal imaging, it is possible to use a radioisotope that emits lower energy photon. ^{125}I decays via electron capture with the emission of a 35 keV gamma ray. Several K shell X-rays with photon energies ranging from 27 to 32 keV from the ^{125}Te daughter product can accompany the decay. The three highest photon emission probabilities for ^{125}I decay are 76% at 27.5 keV, 13% at 31 keV, and 7% at 35 keV [4]. These gamma rays have an average path-length of about 1 cm in soft tissue, which provides a sufficient transmission probability for the photon to escape from the body of the small animal. In addition, ^{125}I has a half-life of 59.4 days, and is already widely used in molecular biology research.

There are a number of advantages of using ^{125}I for small-animal imaging. First, many ^{125}I-labeled nucleic acids, antibodies, ligands, and other radiopharmaceuticals are commercially available [5, 6]. In addition, many other ^{125}I-labeled imaging probes can be readily synthesized using commercial iodination reagents and kits. Second, ^{125}I-labeled biological compounds or imaging probes can be readily replaced with another iodine radioisotope without changing their chemical and biological properties. One possible replacement is ^{123}I, which emits a higher photon energy (159 keV) that is more appropriate for SPECT imaging in humans. Another possible replacement is ^{124}I, which is a positron emitter that allows the use of PET imaging. The ability to directly translate the research and techniques developed from small-animal imaging to clinical use is an important advantage. Finally, the long half-life makes radiolabeling

work more convenient and also permits the study of gene expression products to be performed over an extended period of time in the same animal. However, in some cases, such long half-life can pose a problem because the iodine stays in the animal and continues to emit a strong signal, making repeat studies difficult. In instances where a short half-life of the radioisotope is needed, one possible solution is to replace ^{125}I with ^{123}I, which has a half-life of 13.2 hours. ^{123}I has a gamma-ray emission at 159 keV, but also results in the emission of the K shell X-rays of the ^{125}Te daughter product in the 27–32 keV range. For these reasons, *in vivo* ^{125}I imaging in small animals is very attractive and has motivated several groups to develop dedicated systems toward this goal [7-12].

III. Si(Li) Detectors

Although silicon (Si) is not normally considered for use as gamma-ray detection because of its low density and atomic number, its properties are quite favorable for ^{125}I imaging. Because of the low-energy emissions of ^{125}I, Si has similar absorption length for 27 keV photons (~2.36 mm) as CsI(Tl) has for 140 keV photons. In addition, Si also has adequate photoelectric fraction (80%) for the emissions of ^{125}I. While detectors fabricated from high-resistivity Si are already commercially available, their thickness is limited to a maximum of about 2 mm. In order to get good detection efficiency (~90%), the thickness of the silicon has to be greater than 5 mm. Thicker detectors can be achieved by using lithium-drifted silicon (Si(Li)) detectors. The process of drifting lithium into the silicon compensates for the impurities in silicon, thereby creating a bulk of "intrinsic" silicon, which can be made up to 1 cm thick. Si(Li) detectors have been made for over 40 years. The physics is very well understood and the basic fabrication process is a very mature technology. Other advantages of using Si(Li) include the ability to fabricate large active area detectors (10 cm × 10 cm) and the availability of many resources for processing silicon. Improved techniques for fabricating multi-electrode Si(Li) detectors have recently been developed [13]. We believe Si(Li) detectors offer the ideal solution for *in vivo* ^{125}I imaging.

Scintillator-based detectors have been used in nuclear imaging since the beginning of the field. Most of the development in conventional gamma camera is optimized for photon energies between 140 keV to 511 keV. The developments in position-sensitive photomultiplier tubes (PSPMTs) and scintillator arrays such as NaI(Tl) and CsI(Tl) have allowed the development of high-resolution compact gamma detectors. However, because of the low-energy emissions of ^{125}I, the energy resolution of a scintillator-based detector is not very good. On the other hand, the direct conversion of the photon energy in a Si(Li) detector yields a large signal, thereby the energy resolution of a Si(Li) detector is very good for the emissions of ^{125}I. Another disadvantage of scintillator-based detectors is the high cost of the PSPMT. Other semiconductor detectors such as germanium (Ge) and cadmium zinc telluride (CdZnTe) detectors also give very good energy resolution. However, Si(Li) detectors offer distinct advantages over these other semiconductor detectors. Operation of Ge detectors requires cryogenic temperature (~77K). Si has higher bandgap than Ge, allowing Si(Li) detectors to be operated at room temperature, which is impossible for Ge detectors because of the large thermally-induced leakage current. On the other hand, CdZnTe is a high Z, wide bandgap semiconductor that allows operation at room temperature with low leakage current. However, the reliable production of a large area CdZnTe detectors (> several cm^2) is fairly difficult due to crystal inhomogeneity and the low yield of single-crystal material. A large active area detector can be constructed by tiling detectors together, but dead area is introduced between the detectors. Another advantage of using Si over CdZnTe is that the energy required to create an electron-hole pair is lower in Si than in CdZnTe, so the signal contribution to the energy resolution in better in Si. Table I compares the properties of Si, Ge, and CdZnTe.

TABLE I
PROPERTIES OF SEMICONDUCTOR MATERIALS AT ROOM TEMPERATURE

Material	Si	Ge	CdZnTe
Atomic number	14	32	48/30/52
Energy gap (eV)	1.115	0.746 [b]	1.64
Energy/e-h pair (eV)	3.6	2.96 [b]	5.0
Photoelectric Fraction @ 27 keV	0.84	0.97	0.97
Photoelectric Fraction @ 35 keV	0.74	0.95	0.97
Absorption Length @ 27 keV (mm)	2.36	0.11	0.07
Absorption Length @ 35 keV (mm)	4.45	0.21	0.07
Electron Mobility (cm^2/V.s)	1350	3900	1000-1100 [a]
Hole Mobility (cm^2/V.s)	480	1900	50 [a]
Electron Lifetime (s)	2.5×10^{-3}	$\geq 10^{-4}$ [b]	$0.8\text{-}8 \times 10^{-6}$ [a]
Hole Lifetime (s)	2.5×10^{-3}	$\geq 10^{-4}$ [b]	$60\text{-}600 \times 10^{-9}$ [a]

All numbers are from [14] and [15], except otherwise stated.
[a] Taken from [16].
[b] At 77 K.

IV. System Design

We proposed a design for a high-resolution SPECT system for *in vivo* ^{125}I imaging in small animal using Si(Li) detectors as the gamma-ray imaging detectors. As shown schematically in Fig. 1, the SPECT system consists of a dual head detector geometry that is mounted on a rotating gantry, allowing for the possibility of putting an X-ray CT or an optical imaging system on the other arm. Each detector head consists of a single, pixellated, monolithic Si(Li) detector with an active area of about 64 mm x 40 mm. The detector has high detection efficiency (>90%), good energy resolution (<15% FWHM), and good intrinsic spatial resolution (~1 mm FWHM) for the emissions of ^{125}I.

The design of the detector head is shown in Fig. 2. Each detector head consists of the pixellated Si(Li) detector that is mounted on the detector module board, providing the

electrical connections between the detector and the front-end readout boards. Each front-end readout board has two application-specific integrated circuits (ASICs) to read out the detector signals. Each front-end readout board plugs into a detector head motherboard that provides the control signals, processes the output signals, and sends the data to the computer.

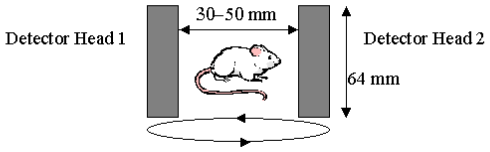

Fig. 1. Proposed dual head SPECT system rotating around the mouse.

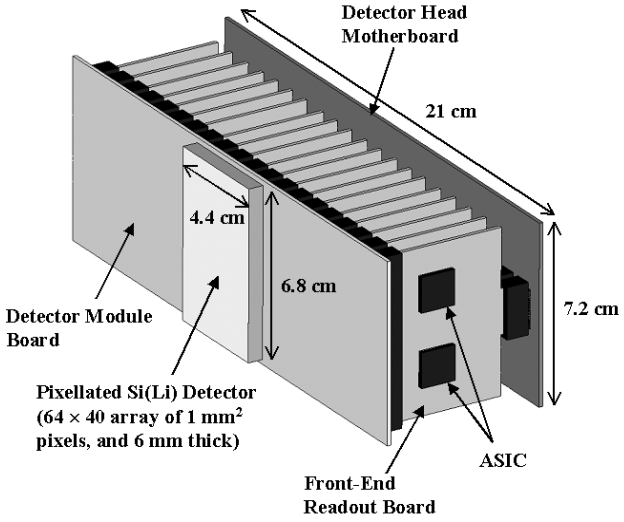

Fig. 2. Design of the proposed detector head.

A. Pixellated Si(Li) Detectors

Each pixellated Si(Li) detector is an array of 64 × 40 pixels, each 1 mm^2 to achieve an intrinsic spatial resolution of 1 mm. The thickness of the detector is 6 mm, which is sufficient (for silicon) to achieve greater than 90% detection efficiency for the emissions of ^{125}I. The detector will be fabricated at Lawrence Berkeley National Laboratory (LBNL) using the standard LBNL Si(Li) process, which has been described in [17, 18]. A new robust contact recently developed at LBNL [13] will be used to segment one side of the detector into a 64 x 40 array of 1 mm^2 pixels. A guard ring structure around the array of pixels will be fabricated to sink surface leakage current.

While Si(Li) detectors are usually cooled in order to reduce the leakage current, the pixel size in this design is small enough to allow room temperature operation. The bulk leakage currents of each pixel is given by [19]

$$I = \frac{qn_iW}{2\tau_o}$$

where q is the equivalent charge (1.6×10^{-19} C), n_i is the intrinsic carrier concentration (1.5×10^{10} cm^{-3} at room temperature), W is the depleted volume (1 mm × 1 mm × 6 mm), and τ_o is the carrier lifetime (about 2.5 ms). The expected bulk leakage current in each pixel is therefore about 3 nA at room temperature. The compensated region of the Si(Li) detector is stable and can be operated at room temperature. However, if necessary, the detector will be cooled to achieve better detector performance.

B. Readout Electronics

We will be using the readout ASIC that we had developed and fabricated for reading out the signals from photodiode arrays [20, 21]. The readout IC is described in detail in [22]. It is a mixed analog-digital design fabricated in CMOS (HP 0.5 μm 3.3 V technology) and covering an area of 4.5 mm x 4.8 mm. Its front-end is an array of 64 analog input channels consisting of charge-sensitive preamplifiers and shaper amplifiers. It is then followed by a "Winner Take All" (WTA) circuitry that reduces the 64 amplified, shaped signals to a single analog signal with the largest amplitude plus 6 digital bits that identify the winning channel. The charge-sensitive preamplifier of the readout ASIC is optimized for a low input load of about 5 pF

C. System Spatial Resolution and Sensitivity

Geometric collimation is employed in gamma camera using parallel-hole or pinhole collimators. However, the collimator is the limiting factor for both the spatial resolution and sensitivity. There has been an enormous interest in pinhole SPECT system for small animal imaging. Pinhole collimators can yield good system spatial resolution for SPECT because the spatial resolution is only weakly dependent on the intrinsic resolution of the detector if the magnification factor is large enough. For a field-of-view (FOV) of the size of a mouse (30 mm to 50 mm), an active area of the detector greater than 15 cm yields a magnification factor greater than 3. Thus, a pinhole collimator coupled to a conventional gamma camera creates an effective mouse imaging system. Short imaging distances are used in pinhole imaging to increase the geometric efficiency of the collimator as shown in Fig. 3, but this also results in a smaller FOV. Parallel-hole collimators, on the other hand, generally do not yield the good spatial resolution that pinhole collimator does (as there is no magnification factor that effectively reduces the intrinsic resolution), but the geometric efficiency and FOV do not depend on imaging distance. With a small enough hole diameter, short enough imaging distance and sufficiently good intrinsic resolution, parallel-hole collimators can achieve good system spatial resolution with reasonable geometric efficiency as shown in Fig. 4. We propose to use a set of high-resolution parallel-hole collimators with square hole width of 0.2 mm and septa width of 0.05 mm, giving a system spatial resolution of 1.6 mm FWHM at an imaging distance of 20 mm, and a geometric efficiency of about 10^{-4}. With a detector efficiency of about 90%, this will give a sensitivity of 6.7 cps/μCi for a dual head camera.

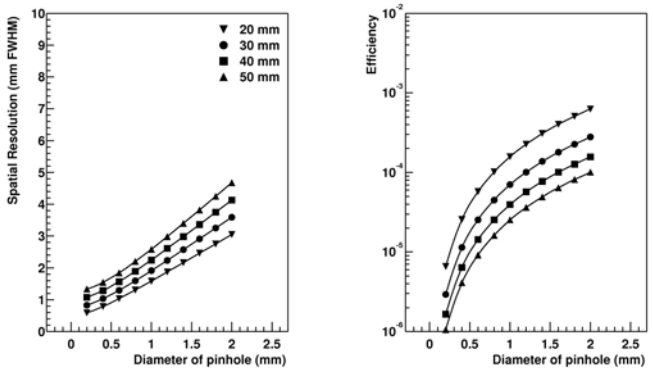

Fig. 3. Spatial resolution and efficiency of a tungsten pinhole collimator as a function of the diameter of the pinhole. The distance from the pinhole aperture to the detector is 40 mm, and the intrinsic resolution of the detector is 1mm. Curves of different imaging distances are plotted.

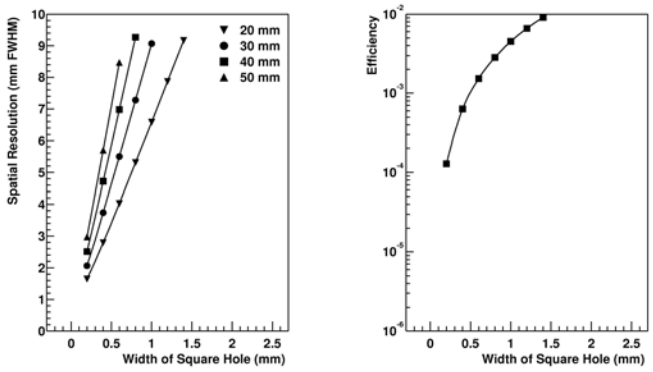

Fig. 4. Spatial resolution and efficiency of a tungsten parallel-hole collimator as a function of the width of the square hole. The geometric length of the collimator is 4 mm, the thickness of the septa is 0.05 mm, the distance of the collimator to the detector is 2 mm, and the intrinsic resolution of the detector is 1mm. Curves of different imaging distances are plotted. Note that the efficiency of parallel-hole collimators is independent of the imaging distance.

As a result of the low geometric efficiency of the collimator, the statistical noise is a major limitation of SPECT system. In order to estimate the minimum number of events needed to obtain a reasonable quality SPECT image, we use the empirical formula derived in [23]. Each of the Si(Li) detectors has 2560 (64 × 40) pixels. Assume that the region of interest occupies 10 pixels and the required contrast is 2-to-1. The root-mean-square (RMS) uncertainty per pixel is set at 20%. With these parameters, the minimum number of events needed is about 1.6 million events. With a 100 μCi injection in a mouse and a system sensitivity of 6.7 cps/μCi, an imaging time of about 60 minutes would be required. The sensitivity of a SPECT system can be improved by using a lower resolution collimator and/or a higher injection dosage, thereby shortening the imaging time and/or improving the statistical noise in the reconstruction.

V. Results

Measurements are made to evaluate the performance of Si(Li) detector in detecting the emissions of ^{125}I. A single element Si(Li) detector fabricated using the standard LBNL process is used in performing the measurements. The detector is cylindrical in shape. The overall diameter is 24 mm, and the thickness is 6 mm. The diameter of the active area is 16.5 mm. The n-type contact consists of diffused lithium, while the p-type contact is a gold surface barrier. The detector is operated at a reverse bias voltage of 700 V. The detector is evaluated in a liquid nitrogen cryostat where the detector is cooled to lower its leakage current. In the measurements presented here, the detector is cooled to the point that a single channel exhibits a leakage current of about 3 nA to simulate the expected bulk leakage current for a 1 mm x 1 mm x 6 mm (the proposed pixel size) detector element at room temperature. The leakage current measurements are made using a picoammeter. The detector signal is read out by a custom low-noise charge-sensitive preamplifier built from discrete components [24] followed by a Tennelec TC 244 shaper amplifier. In a separate measurement, the detector signal is also read out by the readout ASIC described earlier.

Fig. 5 shows the pulse height spectrum for the Si(Li) detector excited with the emissions of ^{125}I. The detector signal is read out by the custom-built discrete preamplifier with a peaking time of about 2 μs and a detector leakage current of 2.8 nA. The three distinct narrow peaks are the 27.5 keV, 31.0 keV and 35.5 keV emissions of ^{125}I. The broad peak at lower energies is due to photons that have scattered in the material around the detector (e.g., the cryostat cold finger), and are subsequently absorbed in the detector. Fig. 6 and Fig. 7 show the signal amplitude and energy resolution as a function of peaking time respectively. At short peaking times (less than 2 μs) there are significant ballistic deficits causing the signal amplitude to be less than that at long peaking times. Therefore, the energy resolution at short peaking times is significantly poorer. The ballistic deficit is eliminated when the peaking time is above 2–3 μs, achieving the best energy resolution (for 27.5 keV) of 8.5% FWHM for leakage currents of 2.8 nA. The energy resolution increases with increasing peaking time because the parallel noise from the leakage current dominates.

In a separate measurement, the custom-built discrete charge-sensitive preamplifier and the Tennelec shaper amplifier are replaced with the readout ASIC. Fig. 8 shows the ^{125}I pulse height spectrum read out by the readout ASIC with a peaking time of 2 μs and a detector leakage current of 2.8 nA. The individual peaks observed in Fig. 5 are significantly broadened, resulting in one single peak. Taking the peak to be 27.5 keV, the energy resolution is 31% FWHM. The degraded energy resolution (compared to the discrete preamplifier) is due to the fact that the readout ASIC is optimized for an input load of 5 pF. The experimental setup is not ideal and introduces a large input capacitance. The total capacitance shunting the input is measured to be 17 pF, degrading the readout ASIC performance and increasing the electronic noise significantly. However, the readout ASIC could easily be redesigned to handle higher input loads, and should achieve the signal-to-noise ratio obtained with the discrete preamplifier, shown in Fig. 5.

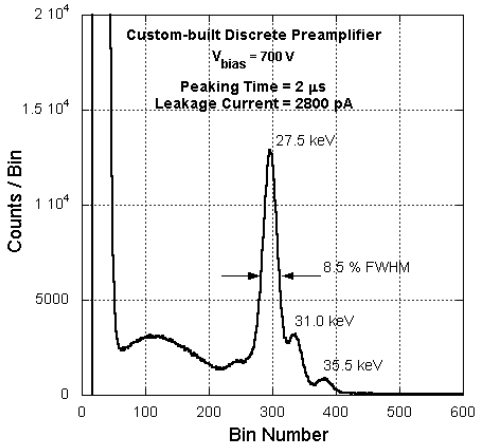

Fig. 5. ^{125}I spectrum read out by the custom-built discrete preamplifier with a peaking time of about 2 μs and a detector leakage current of 2.8 nA.

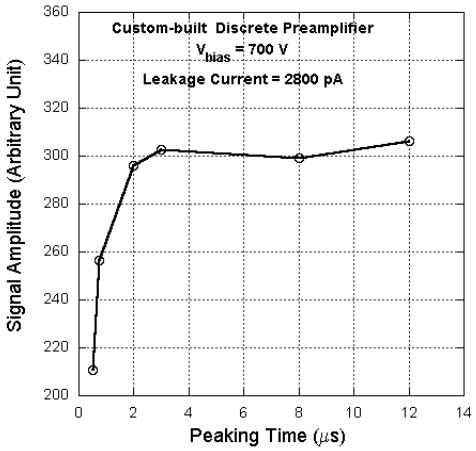

Fig. 6. Signal amplitude of the 27.5 keV emissions of ^{125}I.

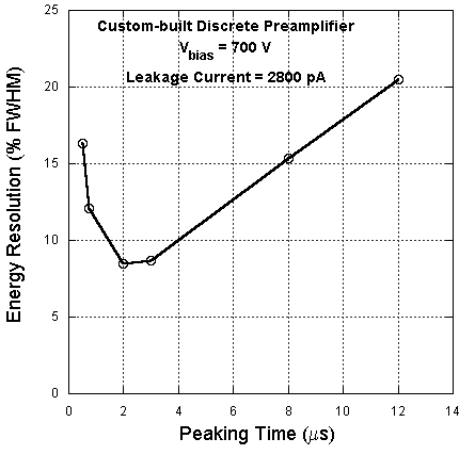

Fig. 7. Energy resolution of the 27.5 keV emissions of ^{125}I.

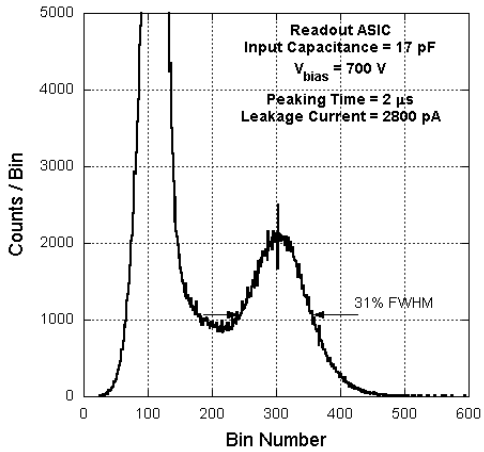

Fig. 8. ^{125}I spectrum read out by the readout ASIC with a peaking time of about 2 μs and a detector leakage current of 2.8 nA. The total capacitance shunting the input of the readout ASIC is measured to be 17 pF.

VI. Conclusions

We have presented a conceptual design for a high-resolution SPECT system using pixellated Si(Li) detectors for *in vivo* ^{125}I imaging. Our results on the detector response to the emissions of ^{125}I show that very good energy resolution can be achieved. Since our readout ASIC is optimized for a low input capacitive load (5 pF), it gives a poor energy resolution because of the large input capacitive load in our experimental setup. However, a minor redesign should yield an ASIC with <10% energy resolution.

VII. References

[1] International Human Genome Sequencing Consortium, "Initial sequencing and analysis of the human genome," Nature, vol. 409, pp. 860-921, 2001.

[2] Mouse Genome Sequencing Consortium, "Initial sequencing and comparative analysis of the mouse genome," Nature, vol. 420, pp. 520-562, 2002.

[3] T. F. Massoud and S. S. Gambhir, "Molecular imaging in living subjects: seeing fundamental biological processes in a new light," Genes and Devel., vol. 17, pp. 545-580, 2003.

[4] S. Y. F. Chu, L. P. Ekstrom, and R. B. Firestone, "WWW Table of Radioactive Isotopes."

[5] NEN Research Products Catalog: PerkinElmer Life and Analytical Sciences, 2003.

[6] Amersham Biosciences Catalog, 2003.

[7] F. A. Dilmanian, D. A. Weber, J. A. Coderre, D. D. Joel, K. G. Shi, G. E. Meinken, et al., "A high resolution SPECT system based on a multichannel-plate imager," IEEE Trans. Nucl. Sci., vol. 37, pp. 687-695, 1990.

[8] K. Iwata, A. B. Hwang, M. C. Wu, H. R. Tang, A. J. Da Silva, K. H. Wong, et al., "Design and utility of a small animal CT/SPECT system," 2001 IEEE Nucl. Sci. Symp. Conf. Rec., vol. 3, 2002.

[9] F. J. Beekman, D. P. McElroy, F. Berger, S. S. Gambhir, E. J. Hoffman, and S. R. Cherry, "Towards in vivo nuclear microscopy: iodine-125 imaging in mice using micro-pinholes," Eur. J. Nucl. Med., vol. 29, pp. 933-938, 2002.

[10] G. A. Kastis, M. C. Wu, S. J. Balzer, D. W. Wilson, L. R. Furenlid, G. Stevenson, et al., "Tomographic small-animal imaging using a high-resolution semiconductor camera," IEEE Trans. Nucl. Sci., vol. 49, pp. 172, 2002.

[11] A. G. Weisenberger, R. Wojcik, E. L. Bradley, P. Brewer, S. Majewski, J. Qian, et al., "SPECT-CT System for Small Animal Imaging," IEEE Trans. Nucl. Sci., vol. 50, pp. 74, 2003.

[12] T. E. Peterson, D. W. Wilson, and H. H. Barrett, “Application of silicon strip detectors to small-animal imaging,” Nucl. Instr. Meth., vol. 505, pp. 608-611, 2003.
[13] I. D. Hau, C. Tindall, and P. N. Luke, "New contact development for Si(Li) orthogonal-strip detector," Nucl. Instr. Meth., vol. A 505, pp. 148-154, 2003.
[14] G. F. Knoll, Radiation Detection and Measurement, 3rd ed. NewYork/Chichester/Weinheim/Brisbane/Singapore/Toronto: John Wiley & Sons, 2000.
[15] S. M. Sze, Physics of Semiconductor Devices, 2nd ed. NewYork/Chichester/Weinheim/Brisbane/Toronto/Singapore: John Wiley & Sons, 1981.
[16] Y. Eisen, A. Shor, and I. Mardor, "CdTe and CdZnTe gamma ray detectors for medical and industrial imaging system," Nucl. Instr. Meth., vol. A 428, pp. 158, 1999.
[17] D. A. Landis, Y. K. Wong, J. T. Walton, and F. S. Goulding, "Computer controlled drifting of Si(Li) detectors," IEEE Trans. Nucl. Sci., vol. 36, pp. 185-189, 1989.
[18] A. Fong, J. T. Walton, E. E. Haller, H. A. Sommer, and J. Guldberg, "Characterization of large diameter silicon low-bias charge collection analysis in Si(Li) PIN diodes," Nucl. Instr. Meth., vol. 199, pp. 623-630, 1982.
[19] A. S. Grove, "Physics and Technology of Semiconductor Devices," Wiley, New York, 1974, pp. 174.
[20] W. W. Moses, J. W. Young, K. Baker, W. Jones, M. Lenox, M. H. Ho, et al., "The electronics system for the LBNL positron emission mammography (PEM) camera," IEEE Trans. Nucl. Sci., vol. NS-48, pp. 632–636, 2001.
[21] G. J. Gruber, W.-S. Choong, W. W. Moses, S. E. Derenzo, S. E. Holland, M. Pedrali-Noy, et al., "A compact 64-pixel CsI(Tl)/Si PIN photodiode imaging module with IC readout," IEEE Trans. Nucl. Sci., vol. NS-49, pp. 147-152, 2002.
[22] M. Pedrali-Noy, G. J. Gruber, B. Krieger, E. Mandelli, G. Meddeler, V. Rosso, et al., "PETRIC - a positron emission tomography readout IC," IEEE Trans. Nucl. Sci., vol. NS-48, pp. 479-484, 2001.
[23] T. F. Budinger, S. E. Derenzo, W. L. Greenberg, G. T. Gullberg, and R. H. Huesman, "Quantitative potentials of dynamic emission computed tomography," J. Nucl. Med., vol. 19, pp. 309-315, 1978.
[24] L. Fabris, "Private communication."